Adaptive Self-Calibrating Parallel Magnetic Resonance Imaging using Kalman Filter

Suhyung Park

Department of Medical Science,

The Graduate School, Yonsei University

Adaptive Self-Calibrating Parallel Magnetic Resonance Imaging using Kalman Filter

Suhyung Park

Department of Medical Science,

The Graduate School, Yonsei University

Adaptive Self-Calibrating Parallel Magnetic Resonance Imaging using Kalman Filter

Directed by Professor Jin Suck Suh

The Master's Thesis submitted to the Department of Medical Science, the Graduate School of Yonsei University in Partial fulfillment of the requirements for the degree of Master of Medical Science

Suhyung Park

December 2010

This certifies that the Master's Thesis
of Suhyung Park is approved.

Thesis Supervisor : Jin-Suck Suh

Thesis Committee Member #1 : Jaeseok Park

Thesis Committee Member #2 : Yong-Min Huh

The Graduate School
Yonsei University

December 2010

ACKNOWLEDGEMENTS

I would like to express my special gratitude to my supervisor, Jin-Suck Suh, who has made me feel comfort in Yonsei University and granted me the privileges to use MR scanner. I am also heartily thankful to my professor, Jaeseok Park, who has taught me everything I know about MR scanners. He not only allows me to explore my interests without getting lost, but also has been the first one to listen to my ideas, and has devoted many hours in helping refine my paper.

There are a few friends who have been supportive along the way. Hyunyeol Lee, my fellow pupil, has encouraged me to be in research and has also continued to be my source of my inspiration. Hahnsung Kim, my senior, has enabled me to develop an understanding of the subject and has been a wonderful mentor, colleague.

Last and most importantly, I offer my regards and blessings to my parents, who have made many sacrifices, and have nurtured me a relentless passion for education.

<TABLE OF CONTENTS>

LIST OF FIGURES

LIST OF TABLES

Adaptive Self-Calibrating Parallel Magnetic Resonance Imaging
using Kalman Filter

Suhyung Park

Department of Medical Science
The Graduate School, Yonsei University

(Directed by Professor Jin Suck Suh)

Parallel magnetic resonance imaging (pMRI) in k-space typically employs variable density sampling and estimates spatial correlation (convolution kernel) among neighboring signals in calibration to reconstruct missing signals. However, it is often challenging to obtain accurate calibration information due to data corruption with noises and spatially varying convolution kernels. Thus, we develop a novel, adaptive self-calibrating pMRI using the Kalman filter, wherein during calibration the variance of estimation errors for convolution kernels is minimized using discrete linear state space models with two distinct phases: predict and update. In the predict phase, convolution kernels and corresponding error covariance at each step are recursively estimated employing an identity state transition model and including process noises (*a priori estimate*). In the update phase, the *a priori* estimates are adaptively estimated between ideal and measured information employing measurement models, which consist of measured signals sliding group-wise with increasing steps to consider spatially varying convolution kernels, and incorporating pre-scanned noises (*a posteriori estimate*). The effect of calibration parameters on the level of artifacts and noises is investigated. Accelerated brain data are reconstructed using both conventional and proposed k-space pMRI for comparison, demonstrating that the proposed method not only produces highly accurate convolution kernels but also reduces artifacts and noises.

Key words: magnetic resonance imaging, partially parallel imaging, self-calibration, adaptive, Kalman filter

I. INTRODUCTION

Partially parallel magnetic resonance imaging (pMRI) techniques[1-18], which exploit coil sensitivity information as supplementary spatial encoding using multiple receiver coils (calibration) to reconstruct missing signals (reconstruction) during data acquisition, have been widely used for rapid MR imaging applications. In pMRI techniques, a fraction of phase encoding (PE) signals, as compared to conventional imaging, are needed, accelerating data acquisition while maintaining spatial resolution. The missing signals are then reconstructed using *a priori* information, spatial variation of coil sensitivity in image-space[1-7] or spatial correlations among neighboring signals in k-space[8-18], calculated during calibration. Thus, it is important to attain highly accurate prior information in calibration to avoid artifacts and noises in image reconstruction.

Calibration signals in pMRI are typically acquired separately before or after actual imaging data (separate calibration)[1-3]. However, the separate calibration potentially results in inconsistency between calibration and imaging data in the presence of subject motions. To alleviate the motion mismatch problems, self-calibration[4-18] is preferred, acquiring both calibration and imaging data simultaneously in a single measurement. Variable density sampling is commonly employed, wherein signals in the central region of k-space are acquired at the Nyquist sampling rate to extract calibration information while those in the periphery of k-space are under-sampled. In image-based SENSE (Sensitivity Encoding)-like pMRI methods[4-7], self-calibration in image-space explicitly calculates coil sensitivity profiles by dividing each coil image, which is generated by performing inverse Fourier transform of the Nyquist sampled central k-space data, by either a root sum of squared magnitudes of all coil images or a uniform body coil image and then smoothing the rough individual coil sensitivity with local polynomial fitting for noise reduction. Since coil sensitivity matrix inversion is performed pixel-by-pixel in reconstruction, image-based self-calibration requires highly accurate coil sensitivity profiles. Thus, a large number of calibration signals in the central region of k-space may be needed, prolonging imaging time. Additionally, in case a reconstructed field-of-view (FOV) is smaller than the object being imaged, image-based self-calibration may yield residual aliasing artifacts in reconstruction[16].

On the other hand, in k-space-based GRAPPA (Generalized Auto-calibrating Partially Parallel Acquisition)-like pMRI methods[8-17], self-calibration calculates spatial correlations

(convolution kernels for reconstruction) between calibration signals and neighboring measured signals directly in k-space by the least squares fitting algorithm. Unlike SENSE-like methods, GRAPPA-like methods need no highly accurate coil sensitivity profiles and have no limitations in the reconstructed FOV. Nevertheless, if data are corrupted with noises or convolution kernels are spatially varying, GRAPPA-like methods lead to residual artifacts and amplified noises spread over the whole image. To mitigate the problems, several self-calibration methods were introduced using: 1) multi-dimensional convolution kernels in k-space, which employ spatial correlations between calibration signals and neighboring multi-column and multi-line (MCML) signals (MCML calibration)[10] , 2) a shift of calibration region from the middle to the periphery of the Nyquist-sampled central k-space (shifted calibration)[9], and 3) an image support reduction with high-pass filtering (HPF calibration)[12]. All of these self-calibration methods obtain partial success but still produce severe artifacts and noises at high acceleration factors. As an alternative, instead of refining self-calibration process, reconstruction in k-space was reformulated incorporating regularization[11] with the prior information extracted from the Nyquist-sampled central k-space. However, the regularization in reconstruction yields a direct tradeoff between image blurring and noise amplification.

To accurately estimate convolution kernels in k-space in the presence of noises, in this work self-calibration in GRAPPA-like methods is reformulated using a discrete linear state space model with spatial and temporal constraints under a framework of the Kalman filter, which incorporates process and measurement noises and thus inherently estimates data-adaptive solution between measured and ideal information, effectively reducing noises without directly sacrificing image sharpness. Spatial variation of correlation among neighboring k-space points is taken into account by updating convolution kernels with increasing steps in the Kalman Filter (KF)[19-20] using measured signals sliding group-wise from the low to high spatial frequency regions. The effect of parameters in the proposed, KF self-calibration method on the level of artifacts and noises in reconstruction is investigated. Accelerated in vivo brain data are reconstructed in k-space using the convolution kernels calculated in: conventional MCML, shifted, HPF, and proposed KF self-calibration, for comparison. It is demonstrated that the proposed, adaptive KF self-calibration not only produces highly accurate convolution kernels in k-space but also reduces residual artifacts and noises even at high acceleration factors.

II. MATERIAL AND METHODS

1. Review of Conventional Self-Calibrating pMRI in k-space

In self-calibrating pMRI[4-18], variable density sampling in k-space is typically employed along the PE direction, wherein low spatial frequency signals are fully sampled while high spatial frequency signals are under-sampled by an outer reduction factor (ORF) (Fig. 1a). Missing signals are reconstructed directly in k-space using pre-defined spatial correlation with their neighboring measured signals. The desired spatial correlation (convolution kernel) is calculated during calibration, in which multiple measured source signals from all coils close to a target calibration signal are linearly combined and then fit to the calibration signal in an individual coil k-space (Fig. 1b):

$$\mathbf{s}_{\gamma}^{\mathbf{CAL}}(\mathbf{k}) = \sum_{\gamma,\mathbf{m}} \mathbf{s}_{\gamma}^{\mathbf{ACC}}(\mathbf{k}')\mathbf{x}_{\mathbf{m},\gamma},\ |\mathbf{k}-\mathbf{k}'| < \mathbf{B} \qquad (1)$$

where γ is the coil index ($\gamma = 1, \ldots, n_c$), n_c is the number of coils, $\mathbf{s}_{\gamma}^{\mathbf{CAL}}(\mathbf{k})$ is the target calibration signal in the Nyquist-sampled central region of k-space for the γ^{th} coil, m is the index for the convolution kernel ($m = 1, \ldots, n_k$), n_k is the length of the convolution kernel for each coil, $\mathbf{s}_{\gamma}^{\mathbf{ACC}}(\mathbf{k}')$ is the measured source signals adjacent to the target calibration signals within the k-space radius (or half the length of a square) B, and $\mathbf{x}_{\mathbf{m},\gamma}$ is the m^{th} element of the convolution kernel to reconstruct missing signals in the γ^{th} coil k-space. Since multiple calibration signals in the central region of k-space are included in the least squares fitting process, Eq. (1) is written as a matrix form:

$$\mathbf{s}_{\gamma}^{\mathbf{CAL}} = \mathbf{s}^{\mathbf{ACC}}\mathbf{x}_{\gamma} \qquad (2)$$

where $\mathbf{s}_{\gamma}^{\mathbf{CAL}}$ is the target calibration signal matrix (n_fx1) for the γ^{th} coil, n_f is the number of target calibration signals, $\mathbf{s}^{\mathbf{ACC}}$ is the corresponding measured source signal matrix ($n_f x n_k n_c$) from all coils, and $\mathbf{x}_{\gamma}$ is the convolution kernel matrix ($n_k n_c$x1) to reconstruct missing signals in the γ^{th} coil k-space. The matrices for $\mathbf{s}_{\gamma}^{\mathbf{CAL}}$ and $\mathbf{s}^{\mathbf{ACC}}$ are filled in a sliding order as shown in Figure 1a in case two-dimensional convolution kernels are employed. The convolution kernels for each coil

k-space are calculated by matrix inversion in Eq. (2).

Assuming that spatial correlation is invariant over the entire k-space, reconstruction in each coil k-space is reduced to the following forward problem using the convolution kernels ($\mathbf{x}_\gamma$) calculated in the central region of k-space during calibration (Fig. 1c):

$$\mathbf{s}_\gamma^{\mathbf{RECON}} = \mathbf{s}^{\mathbf{ACC}}\mathbf{x}_\gamma \qquad (3)$$

where $\mathbf{s}_\gamma^{\mathbf{RECON}}$ is the reconstructed signal matrix for the γ^{th} coil, $\mathbf{s}^{\mathbf{ACC}}$ is the corresponding matrix consisting of measured source signals, which are adjacent to the reconstructed signals, from all coils. Once the missing signals are fully reconstructed, each coil k-space is Fourier transformed, yielding an aliasing-free image. A root sum-of-squares of magnitudes of all the coil images is performed to generate a final, combined image.

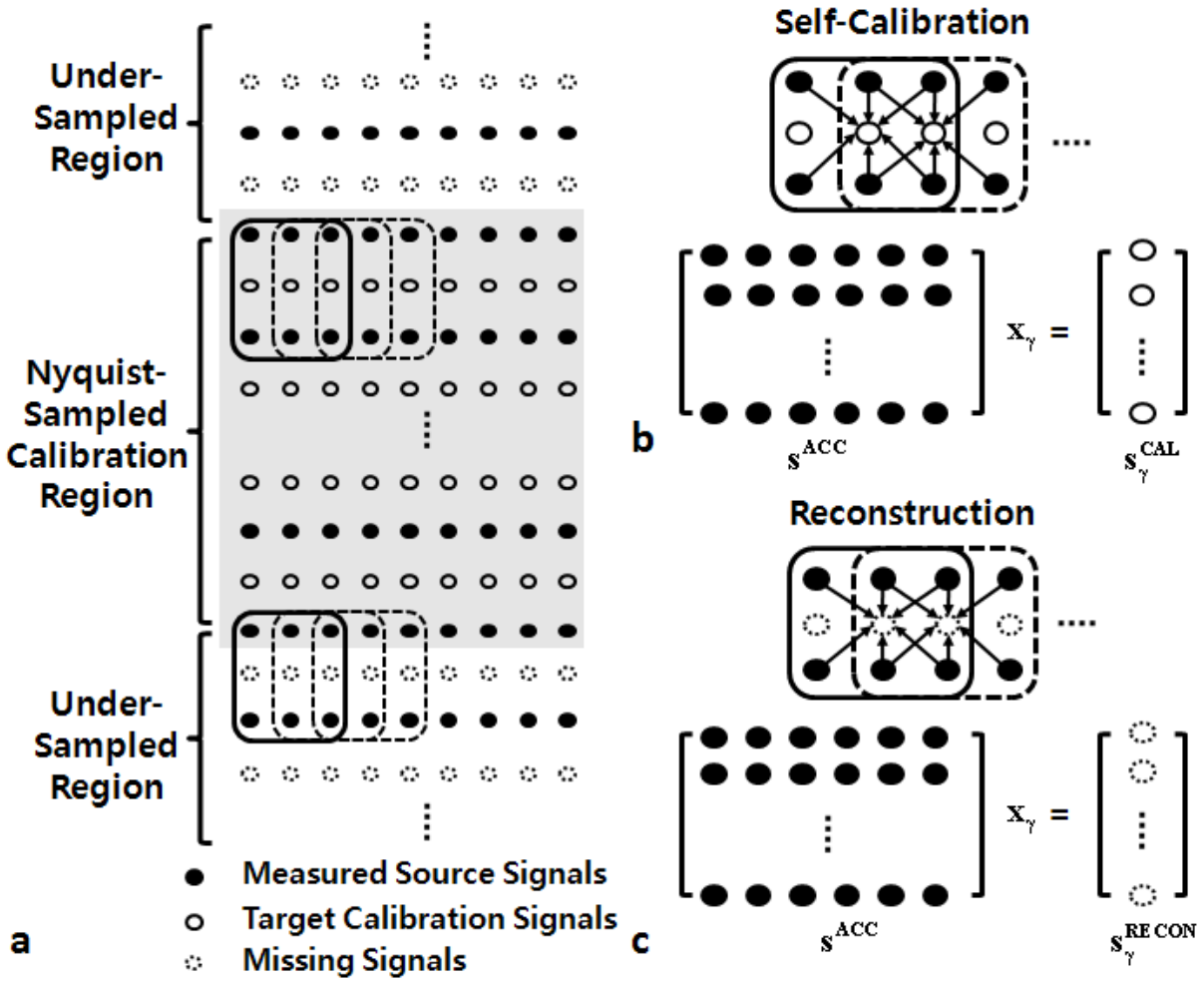

FIG. 1. a: Variable density sampling for self-calibrating pMRI in k-space (ORF = 2), b: Conventional self-calibration to calculate two-dimensional convolution kernels in the Nyquist-sampled calibration region (The matrices for S^{ACC} and S_γ^{CAL} are filled in a sliding order as shown in a), and c: Reconstruction of missing signals in an under-sampled region using the convolution kernels computed during self-calibration (The matrix for S^{ACC} is filled in a sliding order as shown in a). K-space data in the coil dimension is not shown for brevity.

2. Proposed, Adaptive Self-Calibration using Kalman Filter

In conventional self-calibrating pMRI in k-space, it is challenging to accurately estimate convolutions kernels in the presence of noises. Additionally, the underlying assumption, the invariance of spatial correlation, may not be appropriate. That is, the convolution kernels calculated in the central region of k-space may not be optimal in reconstructing missing signals in the peripheral region of k-space[9,17]. Thus, to tackle the problems above, a novel, adaptive self-calibration method in k-space is introduced using a framework of the Kalman Filter, in which during calibration the variance of estimation errors for convolution kernels is minimized using discrete linear state space models with two distinct phases: predict and update.

A. Predict using Discrete Linear State Space Modeling: *a Priori* Estimate

Self-calibration in Eq. (2) is reformulated using the following two discrete linear state space models with pre-defined and measured noises:

$$\text{Process Model : } \hat{\mathbf{x}}_{\gamma,\mathbf{n}}^{-} = \hat{\mathbf{x}}_{\gamma,\mathbf{n}}^{+} + \mathbf{w} \tag{4}$$

$$\text{Measurement Model : } \hat{\mathbf{s}}_{\gamma,\mathbf{n}}^{\mathbf{CAL}} = \mathbf{s}_{\mathbf{n}}^{\mathbf{ACC}} \hat{\mathbf{x}}_{\gamma,\mathbf{n}}^{-} + \mathbf{v} \tag{5}$$

where **n** is the step index, $\hat{\mathbf{x}}_{\gamma,\mathbf{n}}^{-}$ is the estimated convolution kernel matrix ($n_k n_c$x1) for the γ^{th} coil at the n^{th} step, $\mathbf{A_n}$ is the state transition model matrix ($n_k n_c$x$n_k n_c$), $\hat{\mathbf{x}}_{\gamma,\mathbf{n-1}}^{+}$ is the estimated convolution kernel matrix ($n_k n_c$x1) for the γ^{th} coil at the n-1^{th} step, **w** is the process noise matrix ($n_k n_c$x1), $\hat{\mathbf{s}}_{\gamma,\mathbf{n}}^{\mathbf{CAL}}$ is the estimated target calibration signal matrix (n_fx1) for the γ^{th} coil at the n^{th} step, $s_{\mathbf{n}}^{\mathbf{ACC}}$ is the measurement model matrix at the n^{th} step, and **v** is the pre-scanned noise matrix (n_fx1). It is assumed that **v** has a zero mean normal distribution, are statistically mutually independent with w, and are invariant with increasing steps.

Since in theory convolution kernels remain identical with increasing steps due to the linearity of Fourier transform but in practice vary within some uncertainty, in the process model identity state transition model ($\mathbf{A_n} = \mathbf{I_n}$) with the pre-defined process noise (**w**) is employed. In the measurement model, spatial variation of correlation among neighboring k-space points is

taken into account by updating $\mathbf{s}_{\mathbf{n}}^{\mathbf{ACC}}$ with increasing steps using two groups of measured source signals sliding bi-directionally from the central to the peripheral k-space within the Nyquist-sampled calibration region (Fig. 2). A group includes multiple blocks of signals, wherein a block consists of ORF-1 target calibration signals and a measured source signal in the PE direction. Thus, in the update phase that will be introduced in the next section, convolution kernels are accordingly updated but increasingly weighted by measured source signals located in the peripheral calibration region with increasing steps, yielding strong correlations with missing signals in high spatial frequency region.

The uncertainty of the estimated convolution kernels is measured by calculating the error covariance as follows:

$$\mathbf{P}_{\mathbf{n}}^{-} = \mathbf{E}\left[\mathbf{e}_{\mathbf{x}_\gamma,\mathbf{n}}^{-}\mathbf{e}_{\mathbf{x}_\gamma,\mathbf{n}}^{-\mathbf{H}}\right] = \mathbf{E}\left[\left(\mathbf{x}_\gamma - \hat{\mathbf{x}}_{\gamma,\mathbf{n}}^{-}\right)\left(\mathbf{x}_\gamma - \hat{\mathbf{x}}_{\gamma,\mathbf{n}}^{-}\right)^{\mathbf{H}}\right] \tag{6}$$

Replacing $\hat{\mathbf{x}}_{\gamma,\mathbf{n}}^{-}$ by Eq. (4), Eq. (6) is reduced to:

$$\begin{aligned}\mathbf{P}_{\mathbf{n}}^{-} &= \mathbf{A}_{\mathbf{n}}\mathbf{E}\left[\mathbf{e}_{\mathbf{x}_\gamma,\mathbf{n-1}}^{+}\mathbf{e}_{\mathbf{x}_\gamma,\mathbf{n-1}}^{+\mathbf{H}}\right]\mathbf{A}_{\mathbf{n}}^{\mathbf{H}} + \mathbf{E}\left[\mathbf{w}\mathbf{w}^{\mathbf{H}}\right] \\ &= \mathbf{A}_{\mathbf{n}}\,\mathbf{P}_{\mathbf{n-1}}^{+}\,\mathbf{A}_{\mathbf{n}}^{\mathbf{H}} + \mathbf{Q} \\ &= \mathbf{P}_{\mathbf{n-1}}^{+} + \mathbf{Q}\end{aligned} \tag{7}$$

where $\mathbf{x}_\gamma$ is the noise-free measurement convolution kernels, $\mathbf{P}_{\mathbf{n}}^{-}$ is the *a priori* error covariance of convolutions kernels at the n^{th} step, $\mathbf{Q}$ is the step-invariant process noise covariance, which represents the uncertainty of the process model, $\mathbf{A}_{\mathbf{n}}$ is the identity state transition model, and $\mathbf{P}_{\mathbf{n-1}}^{+}$ is the *a posteriori* error covariance of convolution kernels at the $n\text{-}1^{th}$ step. In the predict phase, convolution kernels ($\hat{\mathbf{x}}_{\gamma,\mathbf{n}}^{-}$) and their corresponding error covariance ($\mathbf{P}_{\mathbf{n}}^{-}$) are calculated as *a priori* estimates. As $\mathbf{P}_{\mathbf{n}}^{-}$ reduces, $\hat{\mathbf{x}}_{\gamma,\mathbf{n}}^{-}$ is trusted more.

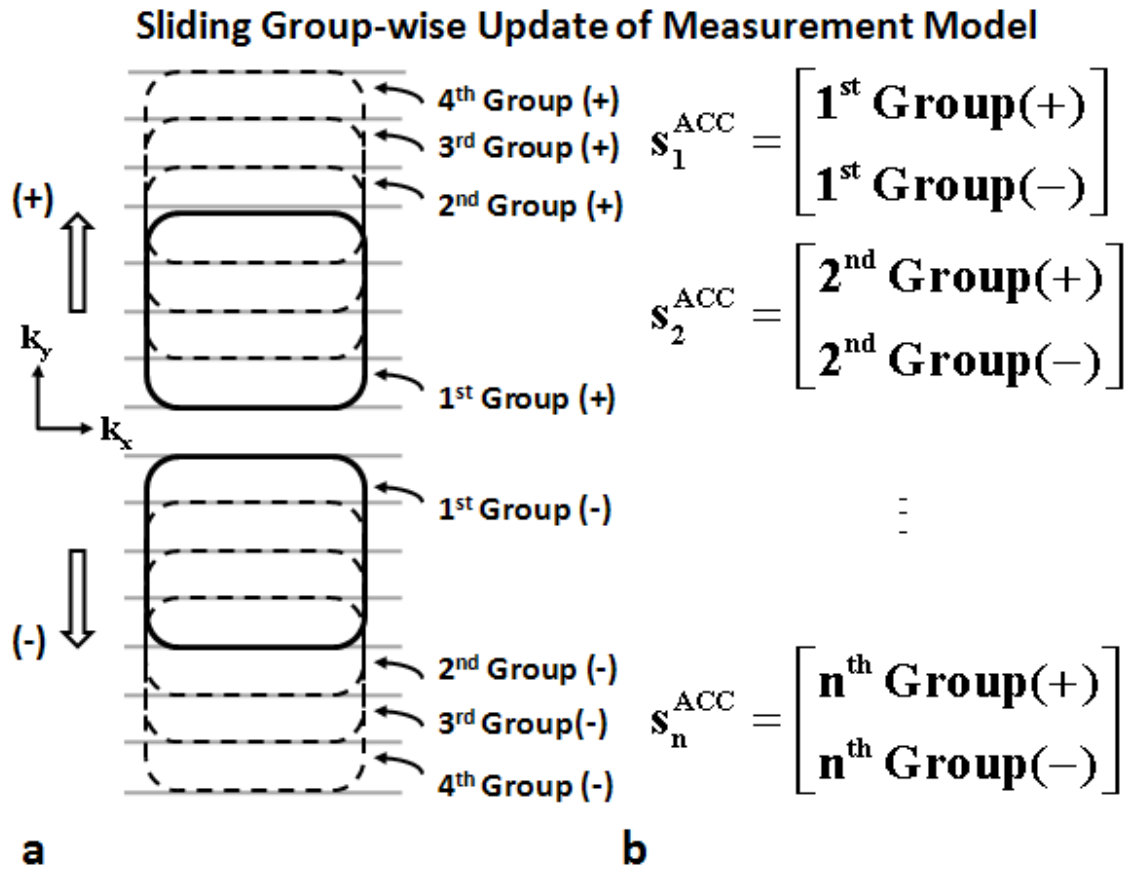

FIG. 2. (a) The proposed measurement model sliding group-wise bi-directionally from the low to high spatial frequency region in k-space with increasing steps, (b) Corresponding measurement model matrix.

B. Optimal Update of Parameters: a Posteriori Estimate

In the update phase, the Kalman filter performs weighted averaging of the predicted and measured states, refining convolution kernels with the following linear recursive formula:

$$\begin{aligned} \hat{\mathbf{x}}_{\gamma,n}^{+} &= \hat{\mathbf{x}}_{\gamma,n}^{-} + \mathbf{K}_n\left(\mathbf{s}_{\gamma,n}^{CAL} - \hat{\mathbf{s}}_{\gamma,n}^{CAL}\right) \\ &= \left(\mathbf{I} - \mathbf{K}_n\mathbf{s}_n^{ACC}\right)\hat{\mathbf{x}}_{\gamma,n}^{-} + \mathbf{K}_n\mathbf{s}_n^{ACC}\mathbf{x}_\gamma \end{aligned} \tag{8}$$

where $\hat{\mathbf{x}}_{\gamma,n}^{+}$ is the *a posteriori* estimate of convolution kernels, $\hat{\mathbf{x}}_{\gamma,n}^{-}$ is the *a priori* estimate of convolution kernels, and $\mathbf{K_n}$ ($n_k n_c x n_f$), which is called the Kalman gain, is the weighted averaging factor between $\hat{\mathbf{x}}_{\gamma,n}^{-}$ and $\mathbf{x}_\gamma$. Eq. (8) suggests that 1) at $\mathbf{K_n} = \mathbf{0}$ the *a posteriori*

estimate of convolution kernels is identical to the *a priori* estimate of convolutions kernels, 2) at $\mathbf{K_n s_n^{ACC}} = \mathbf{I}$ the *a posteriori* estimate of convolution kernels is equal to the noise-free (ideal) measurement convolution kernel, and 3) In neither case, the *a posteriori* estimate of convolution kernels retains an intermediate value between the *a priori* estimate of convolution kernels and the ideal noise-free measurement convolution kernel. Thus, it is important to find an optimal $\mathbf{K_n}$ in the presence of noises.

An optimal $\mathbf{K_n}$ is found by minimizing the error covariance of the *a posteriori* estimate of convolution kernels:

$$\mathbf{P_n^+} = \mathbf{E}\left[\mathbf{e}_{\mathbf{x}_\gamma,\mathbf{n}}^{+}\mathbf{e}_{\mathbf{x}_\gamma,\mathbf{n}}^{+\mathbf{H}}\right] = \mathbf{E}\left[\left(\mathbf{x}_\gamma - \hat{\mathbf{x}}_{\gamma,\mathbf{n}}^{+}\right)\left(\mathbf{x}_\gamma - \hat{\mathbf{x}}_{\gamma,\mathbf{n}}^{+}\right)^{\mathbf{H}}\right] \tag{9}$$

Replacing $\hat{\mathbf{x}}_{\gamma,\mathbf{n}}^{+}$ by Eq. (8), Eq. (9) is reduced to:

$$\mathbf{P_n^+} = \left(\mathbf{1} - \mathbf{K_n s_n^{ACC}}\right)\mathbf{P_n^-}\left(\mathbf{1} - \mathbf{K_n s_n^{ACC}}\right) + \mathbf{K_n R K_n^H} \tag{10}$$

where $\mathbf{R}$ is the measurement noise variance invariant with increasing steps.

$$\frac{\partial \mathbf{P_n^+}}{\partial \mathbf{K_n}} = 2\left(\mathbf{I} - \mathbf{K_n s_n^{ACC}}\right)\mathbf{P_n^-}\left(-\mathbf{s_n^{ACC}}\right)^{\mathbf{H}} + 2\mathbf{K_n R} \tag{11}$$

Setting the derivative of the *a posteriori* estimate of convolution kernels to zero with respect to $\mathbf{K_n}$ results in the following optimal Kalman gain:

$$\mathbf{K_n} = \mathbf{P_n^-}\left(\mathbf{s_n^{ACC}}\right)^{\mathbf{H}}\left(\mathbf{s_n^{ACC}}\mathbf{P_n^-}\left(\mathbf{s_n^{ACC}}\right)^{\mathbf{H}} + \mathbf{R}\right)^{-1} \tag{12}$$

Employing the optimal $\mathbf{K_n}$ in Eq. (12), Eq. (10) is simplified to:

$$\mathbf{P_n^+} = \left(\mathbf{I} - \mathbf{K_n s_n^{ACC}}\right)\mathbf{P_n^-} \tag{13}$$

Detailed derivations of Equations (10) and (13) are described in Appendix. Eq. (12) suggests that 1) if $\mathbf{P_n^-}$ is very small (a high trust in $\hat{\mathbf{x}}_{\gamma,\mathbf{n}}^{-}$), which yields $\mathbf{K_n} \approx 0$, $\hat{\mathbf{x}}_{\gamma,\mathbf{n}}^{+}$ becomes identical to $\hat{\mathbf{x}}_{\gamma,\mathbf{n}}^{-}$ while $\mathbf{x}_{\gamma,\mathbf{n}}$ is ignored, 2) if $\mathbf{R}$ is negligible, which leads to $\mathbf{K_n S_n^{ACC}} \approx \mathbf{I}$, $\hat{\mathbf{x}}_{\gamma,\mathbf{n}}^{+}$ is determined solely by $\mathbf{x}_{\gamma,\mathbf{n}}$ without regard to $\hat{\mathbf{x}}_{\gamma,\mathbf{n}}^{-}$, and 3) since $\mathbf{K_n}$ comprises a pseudo inverse of $\mathbf{R}$, the higher $\mathbf{R}$ is the smaller $\mathbf{K_n}$ is. Thus, the elements of $\hat{\mathbf{x}}_{\gamma,\mathbf{n}}^{+}$ for noisy coils (high noise variance) are little weighted, eventually yielding noise reduction with increasing steps.

C. Comparison of the Kalman Filter with Tikhonov Regularization

The optimality criterion of the Kalman filter is to minimize the *a posteriori* estimate of the error covariance of convolution kernels:

$$\min \mathbf{P}_{\mathbf{n}}^{+} = \min \mathbf{E}\left[\left(\mathbf{x}_{\gamma} - \hat{\mathbf{x}}_{\gamma,\mathbf{n}}^{+}\right)\left(\mathbf{x}_{\gamma} - \hat{\mathbf{x}}_{\gamma,\mathbf{n}}^{+}\right)^{\mathbf{H}}\right] \tag{14}$$

Replacing $\hat{\mathbf{x}}_{\gamma,\mathbf{n}}^{+}$ by Eq. (8), Eq. (14) is rewritten as:

$$\min \mathbf{P}_{\mathbf{n}}^{+} = \min \mathbf{E}\left[\left(\mathbf{x}_{\gamma} - \hat{\mathbf{x}}_{\gamma,\mathbf{n}}^{-} - \mathbf{K}_{\mathbf{n}}\left(\mathbf{s}_{\gamma}^{\mathrm{CAL}} - \mathbf{s}_{\mathbf{n}}^{\mathrm{ACC}}\hat{\mathbf{x}}_{\gamma,\mathbf{n}}^{-}\right)\right)\left(\mathbf{x}_{\gamma} - \hat{\mathbf{x}}_{\gamma,\mathbf{n}}^{-} - \mathbf{K}_{\mathbf{n}}\left(\mathbf{s}_{\gamma}^{\mathrm{CAL}} - \mathbf{s}_{\mathbf{n}}^{\mathrm{ACC}}\hat{\mathbf{x}}_{\gamma,\mathbf{n}}^{-}\right)\right)^{\mathbf{H}}\right] \tag{15}$$

$$\begin{aligned} = \min\Bigg\{\mathbf{E}\Big[&\left(\mathbf{x}_{\gamma} - \hat{\mathbf{x}}_{\gamma,\mathbf{n}}^{-}\right)\left(\mathbf{x}_{\gamma} - \hat{\mathbf{x}}_{\gamma,\mathbf{n}}^{-}\right)^{\mathbf{H}} + \mathbf{K}_{\mathbf{n}}\left(\mathbf{s}_{\gamma}^{\mathrm{CAL}} - \mathbf{s}_{\mathbf{n}}^{\mathrm{ACC}}\hat{\mathbf{x}}_{\gamma,\mathbf{n}}^{-}\right)\left(\mathbf{s}_{\gamma}^{\mathrm{CAL}} - \mathbf{S}_{\mathbf{n}}^{\mathrm{ACC}}\hat{\mathbf{x}}_{\gamma,\mathbf{n}}^{-}\right)^{\mathbf{H}}\mathbf{K}_{\mathbf{n}}^{\mathbf{H}}\Big] \\ &-\mathbf{E}\Big[\left(\mathbf{x}_{\gamma} - \hat{\mathbf{x}}_{\gamma,\mathbf{n}}^{-}\right)\mathbf{v}^{\mathbf{H}}\mathbf{K}_{\mathbf{n}}^{\mathbf{H}} + \mathbf{K}_{\mathbf{n}}\mathbf{v}\left(\mathbf{x}_{\gamma} - \hat{\mathbf{x}}_{\gamma,\mathbf{n}}^{-}\right)^{\mathbf{H}}\Big]\Bigg\} \end{aligned} \tag{16}$$

Assuming that the measurement noises ($\mathbf{v}$) and convolution kernel errors ($\mathbf{x}_{\gamma} - \hat{\mathbf{x}}_{\gamma,\mathbf{n}}^{-}$) are statistically independent, the last two terms in Eq. (16) can be ignored. Thus Eq. (16) is reduced to:

$$\min \mathbf{P}_{\mathbf{n}}^{+} = \min \mathbf{E}\left[\left(\mathbf{x}_{\gamma} - \hat{\mathbf{x}}_{\gamma,\mathbf{n}}^{-}\right)\left(\mathbf{x}_{\gamma} - \hat{\mathbf{x}}_{\gamma,\mathbf{n}}^{-}\right)^{\mathbf{H}} + \mathbf{K}_{\mathbf{n}}\left(\mathbf{s}_{\gamma}^{\mathrm{CAL}} - \mathbf{s}_{\mathbf{n}}^{\mathrm{ACC}}\hat{\mathbf{x}}_{\gamma,\mathbf{n}}^{-}\right)\left(\mathbf{s}_{\gamma}^{\mathrm{CAL}} - \mathbf{s}_{\mathbf{n}}^{\mathrm{ACC}}\hat{\mathbf{x}}_{\gamma,\mathbf{n}}^{-}\right)^{\mathbf{H}}\mathbf{K}_{\mathbf{n}}^{\mathbf{H}}\right] \tag{17}$$

$$= \min\left[\left\|\mathbf{x}_{\gamma} - \hat{\mathbf{x}}_{\gamma,\mathbf{n}}^{-}\right\|^{2} + \mathbf{K}_{\mathbf{n}}\left\|\mathbf{s}_{\gamma}^{\mathrm{CAL}} - \mathbf{s}_{\mathbf{n}}^{\mathrm{ACC}}\hat{\mathbf{x}}_{\gamma,\mathbf{n}}^{-}\right\|^{2}\mathbf{K}_{\mathbf{n}}^{\mathbf{H}}\right] \tag{18}$$

where the first term represents a constraint and the second one delineates data fidelity.
Eq. (18) suggests that the optimality criterion of the Kalman filter, if there is no evolution of convolution kernels with increasing steps, is different to the solution of the constrained least squares problem in a sense of the Tikhonov regularization [21]. Since in the Kalman filter the optimal parameter, $\mathbf{K}_{\mathbf{n}}$, is recursively estimated at each step and approaches to the solution with increasing steps between ideal and measured information while in the Tikhonov regularization the solution parameter is held between measured and in accurate prior information, Eq. (18) can be interpreted as an advanced version of the Tikhonov regularization.

D. Implementation of the Proposed KF Self-Calibration in the Nyquist Sampled Calibration Region

A schematic of the proposed KF self-calibration in k-space pMRI is demonstrated in

Figure 3. The initial *a priori* estimates of $\hat{\mathbf{x}}_{\gamma,0}^{+}$ and $\mathbf{P}_{0}^{+}$ are set to zeros and the process noise, $\mathbf{w}$, is set to be small but nonzero at each iteration. In the predict phase, convolution kernels at the current step ($\hat{\mathbf{x}}_{\gamma,n}^{-}$) are estimated by combining those at the previous step ($\hat{\mathbf{x}}_{\gamma,n-1}^{+}$) and the pre-defined process noise ($\mathbf{w}$), and target calibration signals ($\hat{\mathbf{s}}_{\gamma,n}^{CAL}$) are then calculated using the measurement model in k-space ($\mathbf{s}_{n}^{ACC}$) and the pre-scanned measurement noises ($\mathbf{v}$). The measurement model at the 1st iteration ($\mathbf{s}_{1}^{ACC}$) is composed of two blocks of signals in the center of k-space. The uncertainty of the estimated convolution kernels at the current step ($\mathbf{P}_{n}^{-}$) is calculated by adding those at the previous step ($\mathbf{P}_{n-1}^{+}$) to the process noise covariance.

In the update phase, the Kalman gain ($\mathbf{K}_{n}$) is computed at each iteration step using the *a priori* error covariance of convolution kernels, $\mathbf{P}_{n}^{-}$, as well as the measurement parameters, $\mathbf{s}_{n}^{ACC}$ and $\mathbf{R}$. The *a priori* convolution kernels are then combined with the Kalman gain adjusted residuals between target calibration signals and their corresponding estimated calibration signals ($\mathbf{s}_{\gamma,n}^{CAL} - \hat{\mathbf{s}}_{\gamma,n}^{CAL}$), refining the *a posteriori* convolution kernels. The uncertainty of the *a posteriori* estimate of convolution kernels is estimated as Eq. (13). Before moving to the next step, a sliding block-wise update of the measurement model ($\mathbf{s}_{n+1}^{ACC}$) and the target calibration signals ($\mathbf{s}_{\gamma,n+1}^{CAL}$) is performed. Then, it is checked whether or not both the measurement matrices are within the Nyquist-sampled calibration region. Iteration continues as long as the measurement matrices sliding block-wise from the center to the periphery of k-space are within the calibration region.

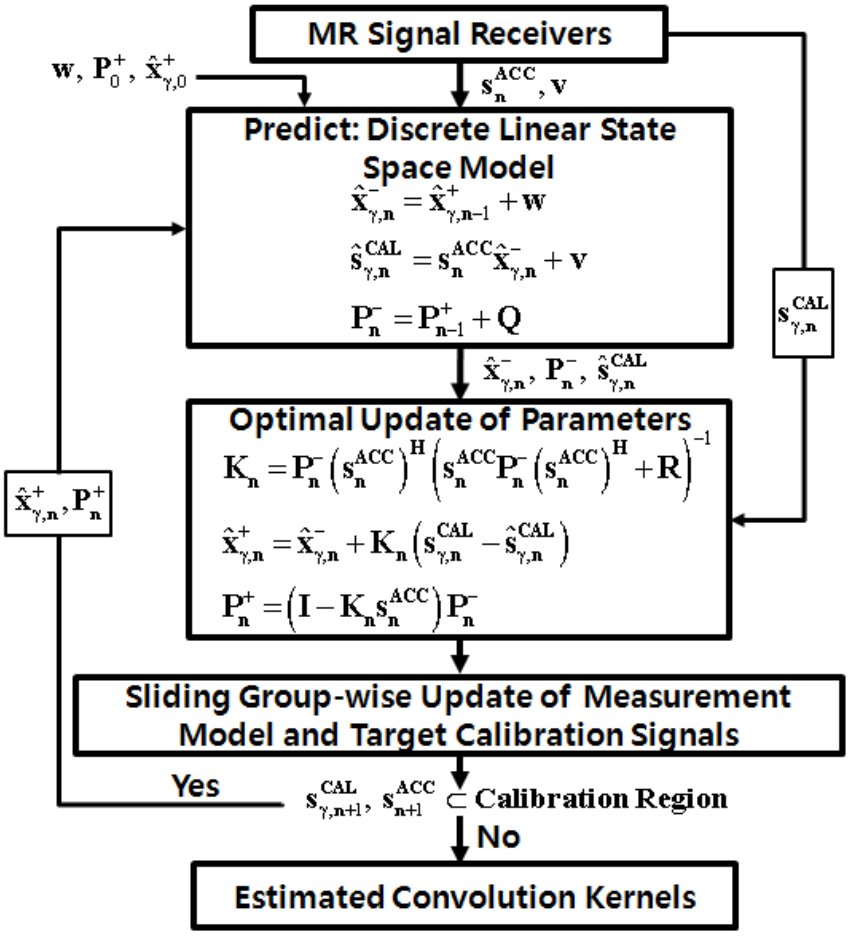

FIG. 3. An overall schematic of the proposed, KF self-calibration in the Nyquist sampled calibration region. In the implementation, two distinct phases (predict and update) are alternated at each iteration, employing sliding group-wise update of measurement model and target calibration signal matrix within the Nyquist-sampled calibration region with increasing steps.

3. Optimization of the Proposed KF Self-Calibration

To investigate the effect of the KF parameters on the level of artifacts and noises in the proposed self-calibrating pMRI, an in vivo brain data is fully acquired in a healthy volunteer using two dimensional (2D) spoiled gradient echo imaging at a 3.0 T whole-body MR scanner (Magnetom Trio, Siemens Medical Solutions, Erlangen, Germany). A twelve-channel head coil is used for signal reception. The imaging parameters are as follows: flip angle (FA), 70^{o}; time-of-echo (TE), 2 ms; time-of-repetition (TR), 22 ms; field-of-view (FOV), $220\text{x}220\text{mm}^2$; slice thickness, 4mm; matrix size, 256x256; and number of average, 1. The fully acquired k-space data is decimated to simulate variable density sampling, wherein the number of the Nyquist-sampled lines (NSL) in the central region of k-space and an ORF in the peripheral region of k-space are adjusted. An off-line image reconstruction for self-calibrating pMRI is performed using the Matlab programming environment (Math Works Inc., Natick, MA).

The optimality of the sliding group-wise measurement model in the proposed KF self-calibration is investigated using the decimated k-space data (ORF, 5; NSL, 40) as compared to: 1) a stationary measurement model which includes signals in the entire calibration region and 2) a stationary shifted measurement model which includes signals partially in the periphery of the calibration region. Images are reconstructed using convolution kernels resulting from the three different measurement models in the proposed KF self-calibration for comparison. Then, the optimal number of blocks (N_B) employed in the sliding group-wise measurement model is estimated with increasing ORF (2, 3, 4) and NSL (16, 32, 48) by calculating the artifact power (AP)[9]:

$$\textbf{Artifact Power (AP)} = \frac{\sum_{\mathbf{j}} \left\| \left|\mathbf{I}_{\mathbf{j}}^{\mathbf{REF}}\right| - \left|\mathbf{I}_{\mathbf{j}}^{\mathbf{RECON}}\right| \right\|^2}{\sum_{\mathbf{j}} \left|\mathbf{I}_{\mathbf{j}}^{\mathbf{REF}}\right|^2} \tag{19}$$

where $\mathbf{j}$ is a pixel index, $\mathbf{I}^{\mathbf{REF}}$ is a reference image, and $\mathbf{I}^{\mathbf{RECON}}$ is an image reconstructed by the proposed KF self-calibration.

To evaluate the effect of the process noise in the proposed KF self-calibration on artifacts and noises, images are reconstructed using four different step-invariant process noise covariance (10^{-6}, 10^{-8}, 10^{-10}, and 10^{-16}) with the following parameters: ORF, 4; NSL, 32; and N_B,

4. With increasing process noise covariance AP is calculated for the following three different sampling parameters: 1) ORF, 4; NSL, 32; 2) ORF, 5; NSL, 40; and 3) ORF, 6; NSL, 48.

To investigate the adaptive solution inherent in the proposed KF self-calibration, noises from all coils are acquired prior to imaging and then incorporated into the measurement model. The KF parameters are: N_B, 2; Q, 10^{-10}; ORF, 6; NSL, 64. Noise variance of each coil is calculated. Convolution kernels for noisy coils (large noise variance), which are estimated using four different calibration methods (conventional MCML[10], shifted[9], HPF[12], and proposed KF self-calibrations), are compared. The resulting convolution kernels are employed to reconstruct missing signals in the peripheral k-space and in the PE direction the reconstructed signals are compared with the corresponding measured signals from the fully acquired data. Images are then reconstructed using the aforementioned four self-calibrating pMRI methods. Residual image artifacts and noises are represented by the absolute difference between the reconstructed and reference images and the geometry factor, respectively. The reference image is obtained by an inverse Fourier transform of the fully acquired coil k-space followed by a root SOS of all the coil images. The geometry factor is quantified[15]:

$$\mathbf{g} = \frac{\mathbf{SNR}^{\mathbf{full}}}{\mathbf{SNR}^{\mathbf{acc}} \cdot \sqrt{\mathbf{R}}} \tag{20}$$

where $\mathbf{g}$ is the geometry factor, $\mathbf{R}$ is the acceleration factor, $\mathbf{SNR}^{\mathbf{full}}$ is the signal-to-noise ratio for fully acquired data, and $\mathbf{SNR}^{\mathbf{acc}}$ is the signal-to-noise ratio for the under-sampled data.

4. In Vivo Comparison between Conventional and Proposed Methods using Actual Accelerated Brain Data

Given the optimal KF parameters in the proposed self-calibrating pMRI, three sets of in vivo brain data are acquired in a healthy volunteer using variable density sampling: 1) ORF, 2; NSL, 16; 2) ORF, 3; NSL, 24; and 3) ORF, 4; NSL, 32. Each set of brain data is reconstructed using conventional MCML, shifted, HPF, and proposed KF self-calibrating pMRI methods for comparison. The KF parameters in the proposed method are: N_B, 4 for ORF=2 and 3, N_B, 2 for ORF=4; Q, 10^{-10}. The imaging parameters are identical to those in the previous section.

Ⅲ. RESULTS

1. Optimization of the Proposed KF Self-Calibration

Figure 4 represents three different measurement models that can be used in the proposed KF self-calibrating pMRI. A stationary measurement model (1st column), which consists of signals in the entire calibration region, results in severe artifacts and amplified noises, since this model does not consider spatial variation of convolution kernels. Compared with the stationary measurement model in the 1st column, a stationary shifted measurement model in the 2nd column, which includes signals partially in the periphery of calibration region, reduces artifacts and noises due to high proximity between calibration and reconstruction regions in k-space. However, residual aliasing artifacts still remain (arrow). A sliding group-wise measurement model in the 3rd column, which includes signals from the central to the peripheral k-space in calibration region with increasing steps, further eliminates residual aliasing artifacts and noises.

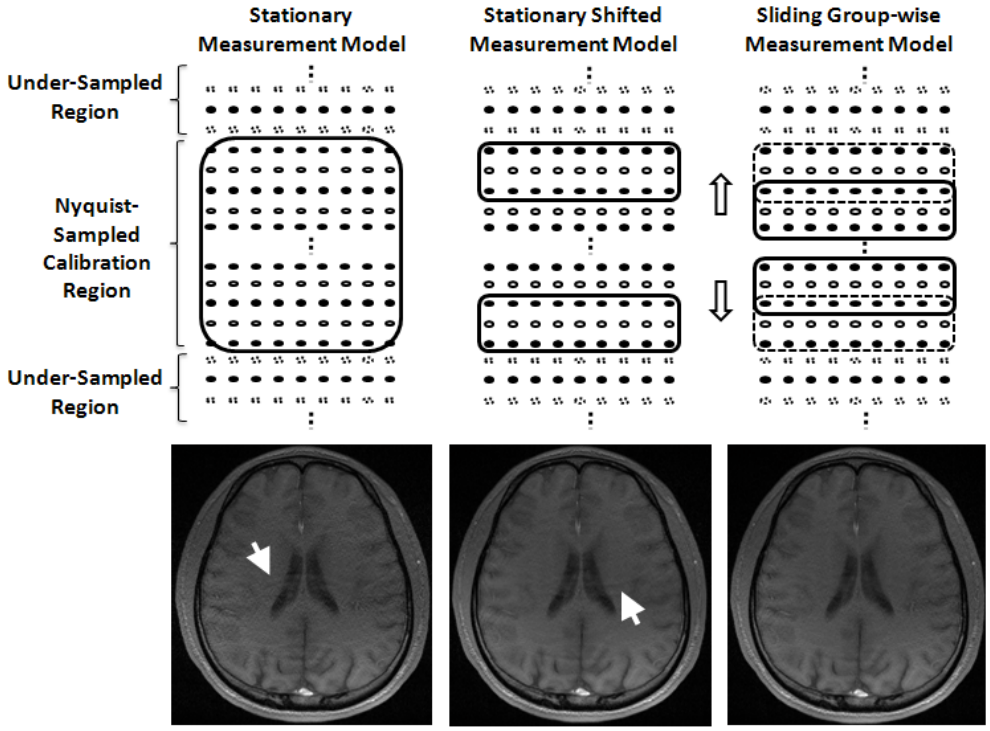

FIG. 4. Top rows: Three different measurement models used in the proposed method: stationary measurement model which includes the entire calibration region (top left), stationary but shifted measurement model which includes only the periphery of calibration region (top middle), and proposed sliding group-wise measurement model with increasing steps (top right), Bottom row: Three corresponding reconstructed images using the top row measurement models (ORF, 5; NSL, 40). Note that artifacts are better suppressed from (a) to (c).

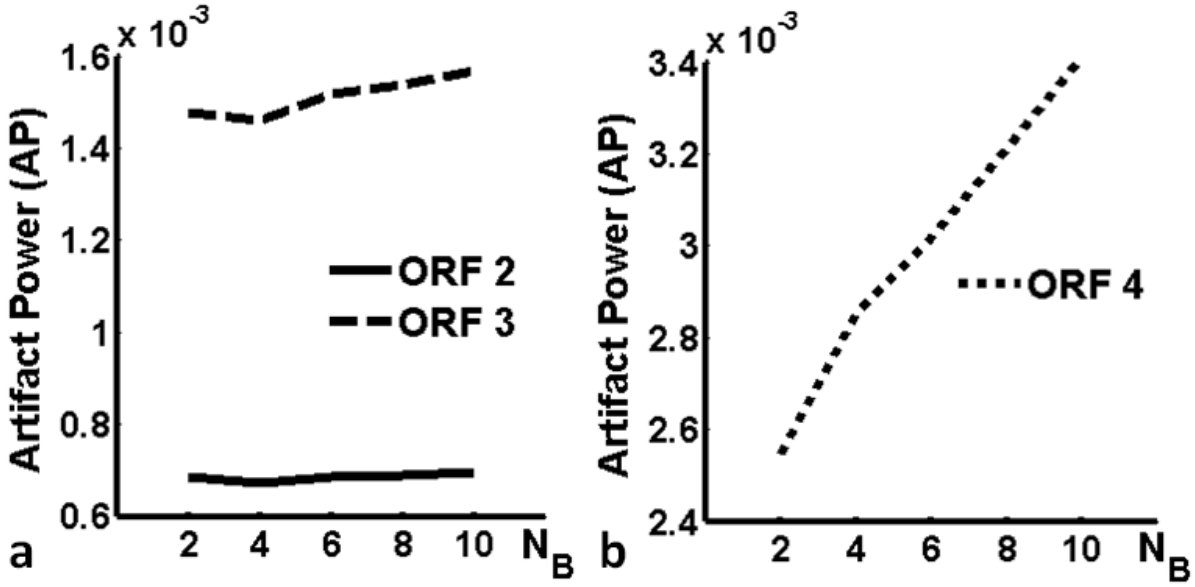

FIG. 5. Artifact power (AP) vs. the number of blocks (N_B) in the sliding group-wise measurement model for the proposed method. Note that at ORF = 2 (NSL, 16) and 3 (NSL, 32) AP reaches a minimal level at $N_B = 4$ while at ORF = 4 (NSL = 48) AP continues to rise with increasing N_B.

Figure 5 illustrates artifact powers calculated with increasing number of blocks in the sliding group-wise measurement model of the proposed KF self-calibrating pMRI for different sampling parameters, ORF = 2, 3, 4 and NSL = 16, 32, 48. When an ORF is set to 2 or 3, AP initially decreases with increasing N_B (≤ 4) while gradually increases at $N_B > 4$. However, AP continues to rise with increasing N_B at ORF = 4. Given the AP calculated with increasing N_B, the optimal N_B is 4 for ORF = 2 and 3 and 2 for ORF = 4.

Given the optimal N_B (2 for ORF=4 and NSL=32), the effect of the step-invariant process noise in the proposed KF self-calibration on image artifacts and noises are shown in Figure 6. Artifacts and noises appear heavily amplified at $Q = 10^{-6}$ (Fig. 6a) and reduce at $Q = 10^{-8}$ (Fig. 6b). As the process noise covariance is decreased to 10^{-10}, artifacts and noises are further reduced (Figs. 6c). However, strong aliasing artifacts result at $Q = 10^{-16}$ due to low data fidelity (Fig. 6d). Figure 7 represents AP with increasing Q for different sampling parameters, ORF = 4, 5, 6 and NSL = 32, 40, 48, respectively. For all the variable density sampling parameters, AP shows a semi-convergence behavior with increasing process noise, wherein AP initially decreases at $Q < 10^{-10}$ while rapidly increases afterwards. Considering data fidelity and noise amplification, an optimal process noise covariance is estimated to 10^{-10}.

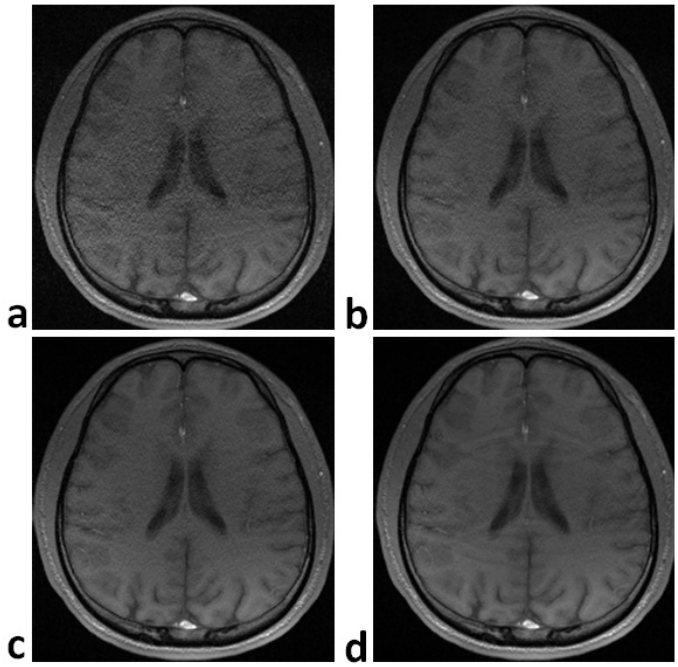

FIG. 6. Images reconstructed using the proposed method (ORF, 4; NSL, 32; N_B, 2) with four different step-invariant process noise covariance (a: 10^{-6}, b: 10^{-8}, c: 10^{-10}, and d: 10^{-16}). Note that image noises decrease (a to c) as the process noise covariance reduces. Also note residual aliasing artifacts at very small process noise covariance (d).

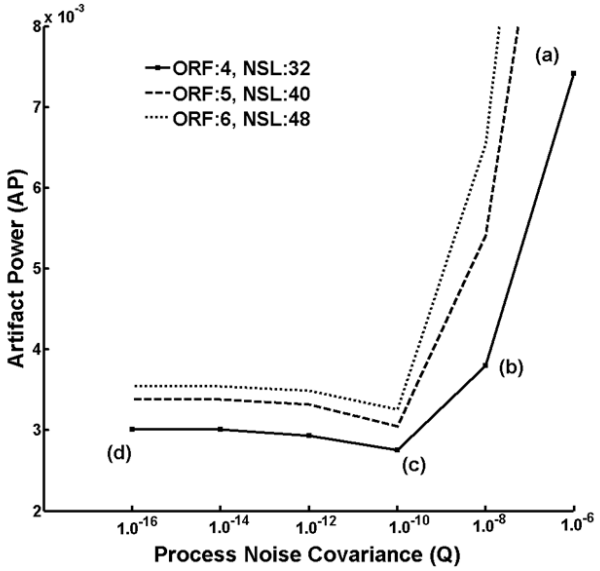

FIG. 7. Artifact power (AP) vs. process noise covariance in the proposed method (N_B=4; thick solid: ORF=2, NSL=24; thin solid: ORF=3, NSL=32; dotted: ORF=4, NSL=48). (a)-(d) indicate the APs which correspond to Fig. 5(a)-(d). Note that with increasing process noise covariance (**Q**) AP slightly decreases at $\mathbf{Q} < 10^{-10}$ while AP rapidly increases afterwards.

Table 1 lists measurement noise variance for all the coils used for data acquisition, representing that coils 9-12 are relatively much noisier than coils 1-8. Given the noise variances in Table 1, the convolution kernels estimated using conventional MCML (Fig. 8a), shifted (Fig. 8b), and HPF self-calibration methods (Fig. 8c) are compared with those calculated using the proposed KF self-calibration method with the optimal KF parameters: $N_B = 2$ and $Q = 10^{-10}$ for ORF = 6 and NSL = 64 (Fig. 8). For coils 1-8 with low noise variances, the convolution kernels calculated using the four self-calibration methods are similar but those resulting from the proposed KF self-calibration vary coil-by-coil the most smoothly. On the other hand, for noisy coils 9-12 coil-by-coil variation of the convolution kernels for conventional MCML, shifted, and HPF self-calibrations is much larger than that for the proposed KF self-calibration, potentially raising weights on noisy signals in reconstruction and thus leading to noise amplification.

TABLE 1. Pre-scanned noise variances for all coils. Note that images are much noisier in coils 9-12 as compared to coils 1-8.

# of Channels	Coil 1	Coil 2	Coil 3	Coil 4	Coil 5	Coil 6	Coil 7	Coil 8	Coil 9	Coil 10	Coil 11	Coil 12
Noise Variance ($\times 10^{-4}$)	1.62	3.01	1.59	2.52	1.9	1.41	4.09	2.91	10.62	34.51	11.85	42.46

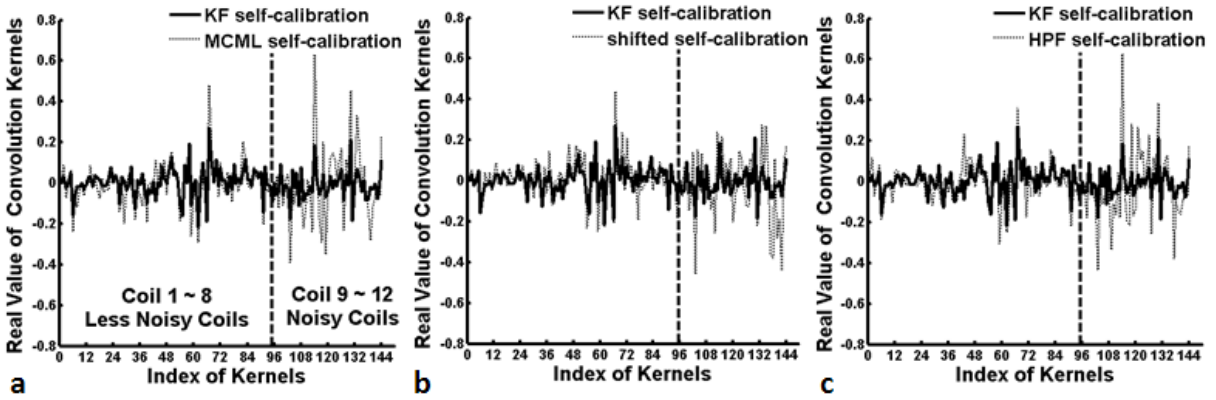

FIG. 8. Comparison of convolutions kernels estimated from: a: conventional MCML self-calibration, b: shifted self-calibration, and c: HPF self-calibration as compared to the proposed KF self-calibration as a reference (thick solid; ORF, 6; NSL, 64; N_B, 2; Q, 10^{-10}). Note that for noisy coils (coil 9-12 as shown in Table 1) the variance of the estimated convolution kernels in (a)-(c) is relatively large as compared to the proposed method.

Missing signals in the PE direction are reconstructed using the convolution kernels resulting from the four self-calibration methods for comparison (Fig. 9). Conventional MCML self-calibration results in high fitting errors in both the low and high spatial frequency regions (Fig. 9a). In the shifted (Fig. 9b) and HPF (Fig. 9c) self-calibration methods, the fitting errors in the low spatial frequency region are reduced but those in the high spatial frequency region still remain severe. The proposed KF self-calibration yields highly accurate reconstruction of missing signals in both the low and high spatial frequency regions (Fig. 9d). The total fitting errors in Figure 9e represent that as compared to conventional MCML self-calibration the accuracy of reconstruction in k-space is improved 23.2 % by the shifted or HPF self-calibration while 41.6 % by the proposed KF self-calibration.

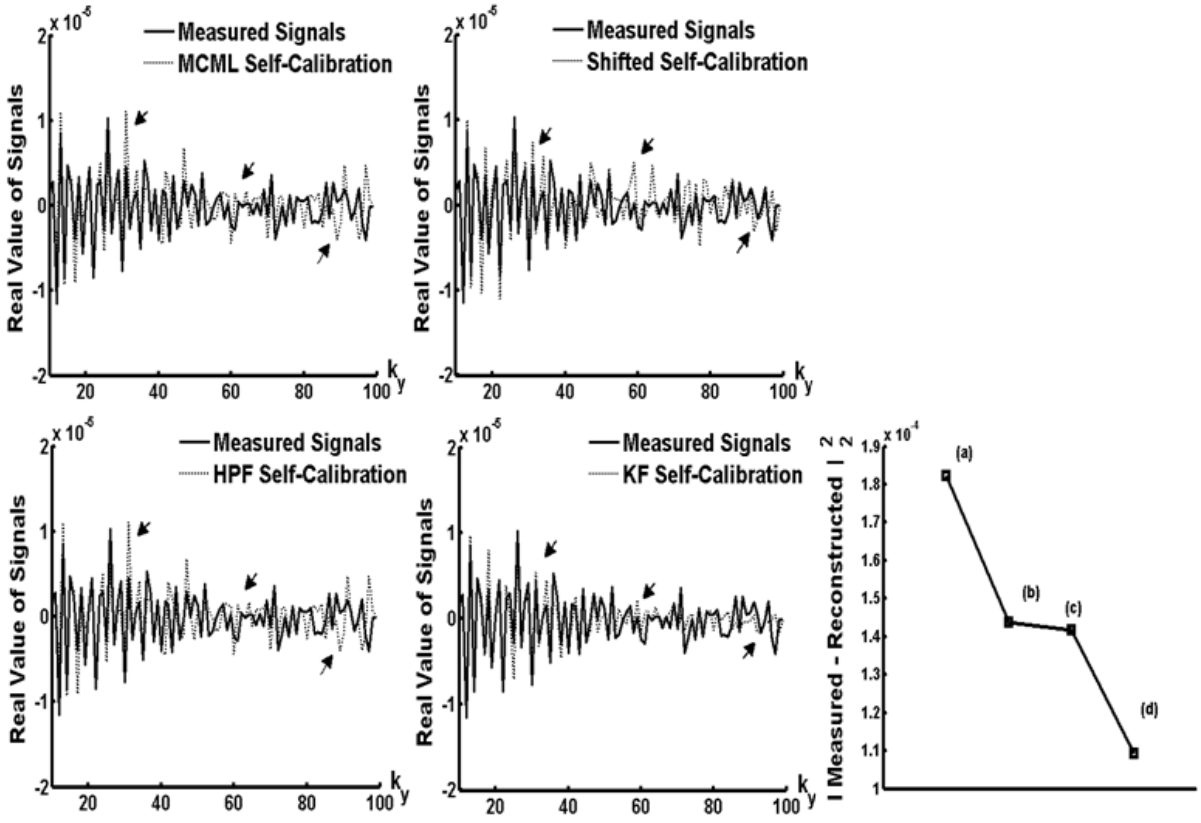

FIG. 9. Comparison of four different k-space signals reconstructed using: a: conventional MCML self-calibration, b: shifted self-calibration, c: HPF self-calibration, d: proposed KF self-calibration, and e: the fitting errors from (a)-(d) (ORF, 6; NSL, 64; N_B, 2; Q, 10^{-10}). Note that the fitting error in (d) is much smaller than (a)-(c).

Given the four different convolution kernels in Figure 8, the corresponding reconstructed images, absolute differences between the reference and reconstructed images, and geometry factor images are compared in Figure 10. Conventional MCML self-calibration (1st column) results in residual artifacts, amplified noises, and high geometry factors over the whole image. The shifted (2nd column) and HPF (3rd column) self-calibration methods decrease residual artifacts and noises but still yield high geometry factors over a large portion of the images. The proposed KF self-calibration (4th column) highly suppresses residual artifacts and noises over the entire image and yields much smaller image difference and lower geometry factors than conventional self-calibration methods (1st-3rd columns).

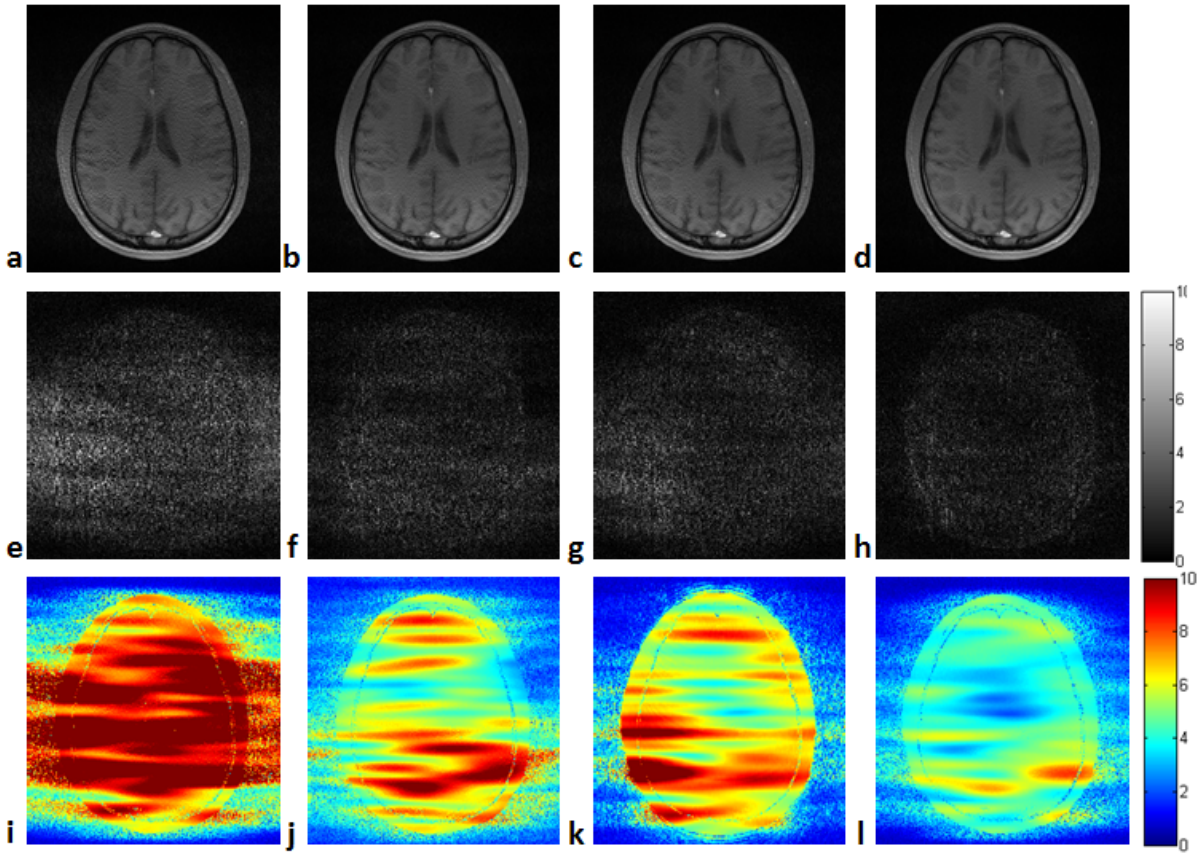

FIG. 10. Comparison of four different self-calibration methods (ORF, 6; NSL, 64). Top row: images reconstructed using conventional MCML (a), shifted (b), HPF (c), and proposed KF self-calibration (N_B, 2; Q, 10^{-10}) (d); Middle row: corresponding difference images between reconstructed and fully sampled reference images (e-h); Bottom row: corresponding geometry factor images (i-l). Note that the proposed

KF self-calibrating pMRI results in much smaller image difference and geometry factor than the other conventional methods.

2. In Vivo Comparison between Conventional and Proposed Methods using Actual Accelerated Brain Data

Figure 11 compares the four brain images acquired using actual variable density sampling (top row: ORF=2, NSL=16; middle row: ORF=3, NSL=24; bottom row: ORF=4, NSL=32) and then reconstructed using conventional MCML (1st column), shifted (2nd column), HPF (3rd column), and proposed KF (4th column) self-calibrating pMRI methods. When an ORF is set to 2 (top row), all the self-calibrations mentioned above result in a low level of residual artifacts and noises (Figs. 11a-11d). As an ORF is increased to 3 (middle row), conventional MCML (Fig. 11e), shifted (Fig. 11f), and HPF self-calibration methods yield artifacts and amplified noises particularly in the central region of image while the proposed KF self-calibration (Fig. 11h) retains a low level of artifacts and noises in the corresponding region. With an ORF of 4 (bottom row), residual artifacts and amplified noises appear in the whole brain image for conventional self-calibration methods (Figs. 11i-11k) while those are substantially reduced in the proposed KF self-calibration method (Fig. 11l). As an ORF is increased, artifacts and noises become rapidly amplified in conventional calibration methods (1st-3rd columns) while those increase slowly in the proposed KF self-calibration method (4th column).

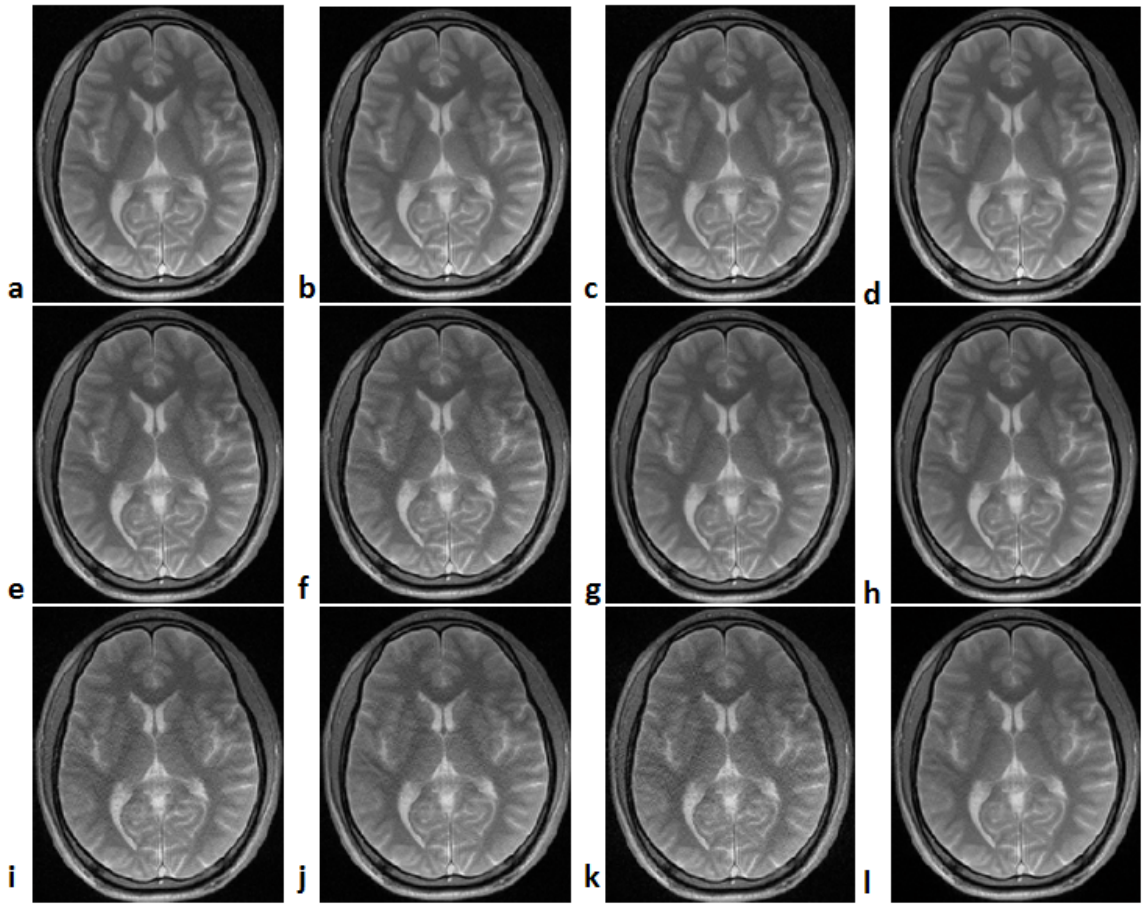

FIG. 11. Comparison of brain images acquired using actual variable density sampling (Top row: ORF=2, NSL=16; Middle row: ORF=3, NSL=24; Bottom row: ORF=4, NSL=32) and reconstructed using four different self-calibration methods (1st column: conventional MCML, 2nd column: shifted, 3rd column: HPF, 4th column: proposed KF (N_B, 4 for ORF=2 and 3, 2 for ORF=4 ; Q, 10^{-10}) self-calibration). Note that compared with conventional self-calibration methods (1st-3rd columns) the proposed KF self-calibration method (4th column) highly reduces residual artifacts and noises at both low and high ORFs.

Ⅵ. DISCUSSION

This work introduces a novel, adaptive self-calibrating pMRI method using a framework of the Kalman filter to accurately estimate convolution kernels in calibration and thus suppress residual aliasing artifacts and noises in reconstruction even at high acceleration factors. The hypothesis of this work is that the errors of convolution kernels in calibration result from data corruption with noises and spatial variation of correlation among neighboring k-space signals. The two sources of calibration errors are not independent and thus need to be addressed together during iterations in the KF self-calibration. At each iteration step, the optimality criterion of the Kalman filter inherently approaches to the solution of a constrained least squares problem between ideal and measured information, wherein the Kalman gain balances data fidelity and noise amplification. Since the Kalman gain includes the inversion of measurement noise variance matrix, convolution kernels for coils with high noise variance are little weighted while those for coils with low noise variance are heavily weighted, yielding coil-dependent weighted convolution and thereby de-noising in image reconstruction. To take into account spatially varying convolution kernels, step-variant measurement models sliding group-wise from the low to high spatial frequency regions with increasing iteration steps are employed, leading to step-variant update parameters in the constrained least squares problem in Eq. (18): Kalman gain ($\mathbf{K_n}$) and prior information ($\hat{\mathbf{x}}_{\gamma,\mathbf{n}}^{-}$). Due to the dynamic nature of the update parameters with increasing steps, the proposed KF self-calibration inherently includes adaptive parameter. Numerical and experimental studies confirm that compared with conventional methods the proposed KF self-calibrating pMRI not only produces accurate convolution kernels in calibration in the presence of noises but also reduces artifacts and noises in reconstruction at high acceleration factors.

Since the full length of convolution kernels requires a long computation time, convolution kernels in self-calibrating pMRI methods are typically truncated and thereby finite convolution kernels are employed to interpolate missing signals in k-space. In the proposed KF self-calibrating method, AP initially decreases with increasing N_B (≤ 4) and then increases afterwards at an ORF of 2 and 3 while AP continues to rise with increasing N_B at an ORF of 4. When an ORF is low and thus spatial correlation between a calibration signal and its neighboring measured signals is strong, with increasing N_B AP initially decreases at $N_B \leq 4$ due to the

reduction of truncation errors in convolution kernels while AP rises at $N_B > 4$ due to numerical instability in calibration resulting from the increased number of unknowns in Eq. (2). However, if an ORF is high and thus spatial correlation between a calibration signal and its neighboring measured signals is weak, AP continues to rise with increasing N_B despite the reduction of truncation errors in convolution kernels. As a result, in the proposed KF self-calibration an intermediate N_B in a sliding group-wise measurement model is optimal for low ORFs while a low N_B is desirable for high ORFs.

A close look at the KF optimality criterion in Eq. (18) suggests that the Kalman gain balances *a priori* information driven constraint (1st term in Eq. (18)) and data fidelity (2nd term in Eq. (18)). With increasing Kalman gain, data fidelity is enhanced but noise-propagation errors are potentially amplified. If the process noise covariance is so small that the error covariance of *a priori* estimate of convolution kernels is low, the Kalman gain is substantially decreased, producing low data fidelity and residual aliasing artifacts in reconstruction (Fig. 6d). On the other hand, in case the process noise covariance is sufficiently large and results in a very high Kalman gain, noise amplification may appear over the whole image (Fig. 6a). Given the considerations above, in this study the process noise covariance, 10^{-10}, is estimated to be optimal for varying sampling parameters. As far as the optimal process noise covariance is chosen, since the inverse of the measurement noise variance is included in the estimation of the Kalman gain, convolution kernels are heavily weighted for coils with low measurement noise variance and little weighted for coils with high measurement noise variance (Fig. 8), resulting in coil-dependent, weighted-averaged de-noising in reconstruction (Fig. 10).

To reduce noise amplification in conventional self-calibrating pMRI, Tikhonov-regularized GRAPPA reconstruction with prior information[11] was introduced by minimizing:

$$\min\left[\left\|\boldsymbol{s}^{ACC}\ \boldsymbol{s}_{\gamma}^{RECON}-\boldsymbol{x}_{\gamma}\right\|_2^2+\lambda\left\|\boldsymbol{s}_{\gamma}^{RECON}-\boldsymbol{s}_{\gamma}^{0}\right\|_2^2\right] \qquad (21)$$

where $\boldsymbol{s}^{ACC}$ is the pseudo-inverse of the measured source signal matrix, λ is the regularization parameter which balances data fidelity (1st term) and prior information driven constraint (2nd term), and $\boldsymbol{s}_{\gamma}^{0}$ is the prior information obtained by performing Fourier transform of the low-resolution images reconstructed using the Nyquist-sampled k-space signals in calibration region. It is assumed that convolution kernels are already given in calibration. Since unlike update gain

of the proposed KF self-calibration the regularization parameter in Eq. (21) is directly multiplied to the constraint term, it suggests that with increasing λ data fidelity is less weighted and residual aliasing artifacts may result while with decreasing λ data fidelity is enhanced but noise propagation errors may be amplified. Image blurring potentially occurs with increasing λ due to the constraint of the low-resolution prior information. Thus, it is challenging to determine an optimal regularization parameter, although there are numerous methods such as truncated singular value decomposition[21], L-curve[21,22], cross validation[21,23]. Additionally, since image reconstruction includes un-regularized pseudo-inverse of $\mathbf{s}^{ACC}$, the solution of Eq. (21) can be numerically unstable. Compared with the Tikhonov-regularized GRAPPA reconstruction, the proposed method is different in that: 1) it incorporates searching-solution into calibration, wherein convolution kernels are obtained by the process noise covariance globally while by the measurement noise variance coil-by-coil, eventually reducing noise amplification in reconstruction; 2) the Kalman gain is adaptively determined and dynamically varies with increasing iteration steps; and 3) since noise reduction is achieved by coil-dependent weighted convolution in reconstruction and no low-resolution prior information is employed, there is no tradeoff between noise amplification and image blurring.

If coil sensitivity is not smooth enough, calibration signals in the central k-space do not represent accurate spatial correlation for missing signals located in the high spatial frequency region. Hence, compared with conventional MCML self-calibration the shifted self-calibration considers spatial variation of correlation among neighboring signals, better suppresses residual aliasing artifacts and noises, as far as the number of NSL is sufficient. If the number of NSL is small, the shifted self-calibration may result in inaccurate convolution kernels because calibration signals are not sufficient in estimating spatial correlation. To resolve this problem, the HPF self-calibration is introduced, employing a high pass filter to suppress high-energy low spatial frequency signals in calibration and thus realizing a concept of image support reduction in k-space. However, the HPF self-calibration is sensitive to pre-defined filter parameters, potentially yielding residual artifacts and amplified noises particularly at high acceleration factors. The proposed KF self-calibration takes into account spatially varying correlation among neighboring k-space signals as in the shifted or HPF self-calibration by employing the sliding group-wise measurement model, and achieves noise reduction efficiently using coil-dependent weighted convolution in reconstruction. In summary, as an ORF increases, residual artifacts and

noises rise rapidly in conventional self-calibration methods while those increase slowly in the proposed KF self-calibration. Thus, the proposed method is robust even at high acceleration factors with a small number of NSL.

In the proposed method, the process noise, which is step-invariant, is included in the predict phase. Since in the proposed measurement model sliding group-wise from the low to high spatial frequency region convolution kernels at a high iteration step are calculated using signals with relatively low SNR, it would enhance the performance of the Kalman filter to employ the step-variant process noise (lower the Kalman gain) decreasing with increasing steps. Additionally, the current proposed KF self-calibration uses the identity state transition model, wherein convolution kernels at the previous step is fully counted while those at the other steps are ignored. However, it would be advantageous to employ a weighted state transition model, in which all the convolution kernels estimated at all the previous steps are taken into account. The step-variant process noise model and the weighted state transition model in the proposed method need to be investigated in the future.

Ⅴ. CONCLUSION

We have demonstrated a novel, adaptive self-calibrating pMRI method using a framework of the Kalman filter. The proposed KF self-calibration method iteratively refines convolution kernels using a step-variant update parameter with the sliding group-wise measurement model, achieving accurate spatial correlation for missing signals in the high spatial frequency region. The proposed KF self-calibrating pMRI in k-space is potentially a promising and efficient solution to reduce residual artifacts and noises even at high acceleration factors.

REFERENCES

[1] K. P. Pruessmann, *et al.*, "SENSE: sensitivity encoding for fast MRI," *Magn Reson Med,* vol. 42, pp. 952-62, Nov 1999.

[2] K. P. Pruessmann, *et al.*, "Advances in sensitivity encoding with arbitrary k-space trajectories," *Magn Reson Med,* vol. 46, pp. 638-51, Oct 2001.

[3] D. K. Sodickson and W. J. Manning, "Simultaneous acquisition of spatial harmonics (SMASH): fast imaging with radiofrequency coil arrays," *Magn Reson Med,* vol. 38, pp. 591-603, Oct 1997.

[4] P. Jakob, *et al.*, "AUTO-SMASH: a self-calibrating technique for SMASH imaging," *Magnetic Resonance Materials in Physics, Biology and Medicine,* vol. 7, pp. 42-54, 1998.

[5] R. Heidemann, *et al.*, "VD-auto-SMASH imaging," *Magnetic Resonance in Medicine,* vol. 45, pp. 1066-74, 2001.

[6] E. Yeh, *et al.*, "3Parallel magnetic resonance imaging with adaptive radius in k-space (PARS): Constrained image reconstruction using k-space locality in radiofrequency coil encoded data," *Magnetic Resonance in Medicine,* vol. 53, pp. 1383-92, 2005.

[7] E. Kholmovski and A. Samsonov, "GARSE: generalized autocalibrating reconstruction for sensitivity encoded MRI," in *Proceedings of the 13th Annual Meeting of ISMRM*, Florida, USA, 2005, p. 2672.

[8] M. Griswold, *et al.*, "Generalized autocalibrating partially parallel acquisitions (GRAPPA)," *Magnetic Resonance in Medicine,* vol. 47, pp. 1202-10, 2002.

[9] J. Park, *et al.*, "Artifact and noise suppression in GRAPPA imaging using improved k-space coil calibration and variable density sampling," *Magnetic Resonance in Medicine,* vol. 53, pp. 186-93, 2004.

[10] Z. Wang, *et al.*, "Improved data reconstruction method for GRAPPA," *Magnetic Resonance in Medicine,* vol. 54, pp. 738-42, 2005.

[11] F. Lin, "Prior-regularized GRAPPA reconstruction," in *Proceedings of the 14th Annual Meeting of ISMRM*, Washington, USA, 2006, p. 3656.

[12] F. Huang, *et al.*, "High-pass GRAPPA: An image support reduction technique for improved partially parallel imaging," *Magnetic Resonance in Medicine,* vol. 59, pp. 642-49, 2008.

[13] T. Zhao and X. Hu, "Iterative GRAPPA (iGRAPPA) for improved parallel imaging reconstruction," *Magnetic Resonance in Medicine,* vol. 59, pp. 903-7, 2008.

[14] Z. Chen, *et al.*, "IIR GRAPPA for parallel MR image reconstruction," *Magnetic Resonance in Medicine,* vol. 63, pp. 502-9, 2009.

[15] F. Breuer, *et al.*, "General formulation for quantitative G-factor calculation in GRAPPA reconstructions," *Magnetic Resonance in Medicine,* vol. 62, pp. 739-46, 2009.

[16] M. Griswold, *et al.*, "Field-of-view limitations in parallel imaging," *Magnetic Resonance in Medicine,* vol. 52, pp. 1118-26, 2004.

[17] F. Huang and G. Duensing, "A theoretical analysis of errors in GRAPPA," in *Proceedings of the 14th Annual Meeting of ISMRM*, Washington, USA, 2006, p. 2468.

[18] C. McKenzie, *et al.*, "Self-calibrating parallel imaging with automatic coil sensitivity extraction," *Magnetic Resonance in Medicine,* vol. 47, pp. 529-38, 2002.

[19] D. Simon, *Optimal state estimation: Kalman, H [infinity] and nonlinear approaches*: John Wiley and Sons, 2006.

[20] N. White, *et al.*, "PROMO: Real-time prospective motion correction in MRI using image-

based tracking," *Magnetic Resonance in Medicine,* vol. 63, pp. 91-105, 2009.
[21] P. Hansen, *Rank-Deficient and Discrete Ill-Posed Problems (Philadelphia, PA: SIAM)*, 1998.
[22] P. Qu*, et al.*, "Discrepancy-based adaptive regularization for GRAPPA reconstruction," *Journal of Magnetic Resonance Imaging,* vol. 24, pp. 248-55, 2006.
[23] R. Nana*, et al.*, "Automatic kernel selection for optimal GRAPPA reconstruction," 2007.

Abstract (In Korea)

칼만 필터를 이용한 적응 셀프 캘리브레이션 병렬 자기 공명 영상 기법

<지도교수 서진석>

연세대학교 대학원 의과학과

박 수 형

k 공간에서 이루어 지는 병렬 자기 공명 영상 기법은 저주파수에 나이퀴스트 샘플링 된 정보를 이용하여 데이터들 간의 상관 관계를 구하고 이 정보를 이용하여 고주파수의 정보를 추정한다. 하지만 노이즈와 k 공간상의 지역적 특성으로 인하여 데이터 간의 정확한 상관 관계를 구하기는 어렵다. 본 논문은 칼만 필터를 이용하여 적응적으로 정규화를 시키는 셀프 캘리브레이션 병열 영상 기법을 제안한다. 칼만 필터는 예측단계와 교정 단계로 이루어진 선형 상태 공간 모델을 이용하여 데이터 간의 상관 관계를 추정한다. 예측 단계에서는 데이터간의 상관 관계와 오차 공분산이 정방 상태 천이 모델과 프로세스 잡음을 이용하여 각 단계에서 반복적으로 추정된다. 교정 단계에서는 예측 단계에서의 추정값이 측정 모델과 측정 잡음을 이용하여 적응적으로 정규화 시킨다. 측정 모델은 각 단계가 진행될수록 저주파수에서 고주파수로 양방향으로 이동시켜 데이터 상관 관계의 가변성을 고려한다. 본 논문은 캘리브레이션 파라미터 변화가 아티펙트와 잡음에 어떤 영향을 미치는지 연구되었고 기존의 방법과의 비교를 위해 실제 병열 데이터를 이용하여 이미지를 재구성 하였다. 본 논문에서 제안된 방법은 정확환 데이터간의 상호관계를 추정할 뿐만 아니라 아티펙트와 잡음 또한 줄일 수 있었다.